The MST4–MOB4 complex disrupts the MST1–MOB1 complex in the Hippo–YAP pathway and plays a pro-oncogenic role in pancreatic cancer

Received for publication, April 2, 2018, and in revised form, July 19, 2018 Published, Papers in Press, August 2, 2018, DOI 10.1074/jbc.RA118.003279

Min Chen[‡], Hui Zhang[‡], Zhubing Shi[‡], Yehua Li[‡], Xiaoman Zhang[‡], Ziyang Gao[‡], Li Zhou[§], Jian Ma[‡], Qi Xu[‡], Jingmin Guan[‡], Yunfeng Cheng[¶], Shi Jiao[‡1], and Zhaocai Zhou[‡§2]

From the [‡]State Key Laboratory of Cell Biology, CAS Center for Excellence in Molecular Cell Science, Shanghai Institute of Biochemistry and Cell Biology, Chinese Academy of Sciences, University of Chinese Academy of Sciences, Shanghai, 200031, the [§]School of Life Science and Technology, ShanghaiTech University, Shanghai 201210, and the [¶]Department of Hematology and Institute of Clinical Science, Zhongshan Hospital, Fudan University, Shanghai 200032, China

Edited by Xiao-Fan Wang

The mammalian STE20-like protein kinase 1 (MST1)–MOB kinase activator 1 (MOB1) complex has been shown to suppress the oncogenic activity of Yes-associated protein (YAP) in the mammalian Hippo pathway, which is involved in the development of multiple tumors, including pancreatic cancer (PC). However, it remains unclear whether other MST–MOB complexes are also involved in regulating Hippo–YAP signaling and have potential roles in PC. Here, we report that mammalian STE20-like kinase 4 (MST4), a distantly related ortholog of the MST1 kinase, forms a complex with MOB4 in a phosphorylation-dependent manner. We found that the overall structure of the MST4–MOB4 complex resembles that of the MST1–MOB1 complex, even though the two complexes exhibited opposite biological functions in PC. In contrast to the tumor-suppressor effect of the MST1–MOB1 complex, the MST4–MOB4 complex promoted growth and migration of PANC-1 cells. Moreover, expression levels of MST4 and MOB4 were elevated in PC and were positively correlated with each other, whereas MST1 expression was down-regulated. Because of divergent evolution of key interface residues, MST4 and MOB4 could disrupt assembly of the MST1–MOB1 complex through alternative pairing and thereby increased YAP activity. Collectively, these findings identify the MST4–MOB4 complex as a noncanonical regulator of the Hippo–YAP pathway with an oncogenic role in PC. Our findings highlight that although MST–MOB complexes display some structural conservation, they functionally diverged during their evolution.

This work was supported by National Key R&D Program of China Grant 2017YFA0504504; National Natural Science Foundation of China Grants 31470868, 81725014, and 91542125; the Youth Innovation Promotion Association of the Chinese Academy of Sciences; "Strategic Priority Research Program" Grant XDB19020202; and China Postdoctoral Science Foundation funded project, 2018T110414. This work was also supported by the SA-SIBS Scholarship Program. The authors declare that they have no conflicts of interest with the contents of this article.

This article contains Figs. S1–S7 and supporting Refs. 1–4.

The atomic coordinates and structure factors (code 5YF4) have been deposited in the Protein Data Bank (http://wwpdb.org/).

[1] To whom correspondence may be addressed: 320 Yue-Yang Rd., Shanghai 200031, China. Tel./Fax.: 86-21-54921291; E-mail: jiaoshi@sibcb.ac.cn.

[2] To whom correspondence may be addressed: 320 Yue-Yang Rd., Shanghai 200031, China. Tel./Fax.: 86-21-54921291; E-mail: zczhou@sibcb.ac.cn.

The Hippo–YAP[3] signaling pathway plays a pivotal role in organ size control and tumorigenesis (1–6). In the mammalian Hippo–YAP pathway, MST1/2 kinases recruit and phosphorylate MOB1, which subsequently interacts with and fully activates LATS1/2 kinases, leading to the phosphorylation and cytoplasmic retention of the downstream transcription coactivator YAP/TAZ (7–10). Recent structural studies of MOB1 interaction with MST1/2 and LATS1/2 also highlight the importance of MOB proteins as kinase adaptors (8). In addition to MOB1A/B, the Mps one binder (MOB) family of proteins include other members like MOB2, MOB3A/B/C, and MOB4 (also known as phocein) in humans. Meanwhile, the mammalian STE20-like (MST) protein kinase family contains not only MST1/2 but also MST3, MST4, and STK25 that are relatively less investigated but sporadically associated with cell proliferation and apoptosis (Fig. 1*A*) (11–15). Furthermore, MOB3A/B/C can associate with and negatively regulate MST1-mediated apoptosis to support tumorigenesis in glioblastoma multiforme (16), indicative of distinct roles of MST–MOB pairing. Currently, however, the physical and functional interplay between MST kinases and MOB adaptors remains only partially understood.

A common feature of the MST kinases lies in their conserved topological structure containing an N-terminal kinase domain, a C-terminal dimerization domain, and a regulatory linker region in between (Fig. 1*A*) (17). Lately, multiple MST kinases, in particular MST1/2 and MST4, have been identified as components of the striatin (STRN)-interacting phosphatase and kinase (STRIPAK) complexes (18–20). Human MOB4, initially identified as an interacting protein of striatins, was also found in the STRIPAK complexes (21, 22). Moreover, a recent study revealed that the STRIPAK complex regulates breast cancer cell

[3] The abbreviations used are: YAP, Yes-associated protein; PC, pancreatic cancer; MOB, Mps one binder; SUMO, small ubiquitin-like modifier; TEV, tobacco etch virus; MBP, maltose-binding protein; MTT, 3-(4,5-dimethylthiazol-2-yl)-2,5-diphenyltetrazolium bromide; MST, mammalian STE20-like; CBB, Coomassie Brilliant Blue; ITC, isothermal titration calorimetry; BLI, bio-layer interferometry; PDB, Protein Data Bank; IHC, immunohistochemistry; shRNA, short hairpin RNA; λPP, λ protein phosphatase; STRIPAK, striatin-interacting phosphatase and kinase; TMA, tissue microarray; STRN, striatin; FBS, fetal bovine serum; DMEM, Dulbecco's modified Eagle's medium.

migration and metastasis by controlling the activity of MST kinases (23). Thus, MST kinases and MOB proteins, as individual molecules or part of the STRIPAK complexes, could be involved in the development of various tumors, including pancreatic cancer (PC) (24). Yet, the possible pairing between MSTs and MOBs, as well as their specific functions in PC, remains unknown.

MST4 was previously reported to act downstream of the tumor suppressor kinase LKB1 for cell polarity control in gut (25, 26). Emerging evidence points to an important role of MST4 in tumorigenesis, including breast cancer, prostate cancer, and glioblastoma (23, 27, 28). The activity and subcellular localization of MST4 are differentially regulated in various biological processes. For example, MST4 can localize at the Golgi apparatus through its association with the Golgi matrix protein GM130 to regulate Golgi morphology and control cell migration (29). CCM3 was also found to form a complex with MST4 and GM130 on the Golgi apparatus to stabilize MST4 (30). Meanwhile, it appears that STRN cannot only negatively regulate the activation of MST4 but also facilitate its Golgi localization (20, 31, 32). It is speculated that MST4 might be physically and functionally associated with other components of the STRIPAK complex such as MOBs and other MST kinases. Additionally, recent studies indicated that components of STRIPAK complex are emerging regulators of Hippo signaling pathway (33–35). To date, however, it remains unclear whether MST4 can also use MOBs to regulate MST1 and thus Hippo–YAP signaling.

Previously, we have identified the MST4 kinase as a dynamic inhibitor of the Toll-like receptor pathway that directly phosphorylates the signaling adaptor TRAF6 during inflammation (36), and we revealed the regulatory mechanisms of MST4 by MO25 (12) and CCM3 (37). Here, in dissecting the potential interplay between MST kinases and MOB adaptors, we identified an MST4–MOB4 complex structurally reminiscent of the MST1–MOB1 complex but with opposite biological function in PC. MST4 interacts with MOB4 in a phosphorylation-dependent fashion to form a complex that synergistically promotes PC cell proliferation and migration. The MST4–MOB4 complex interferes with the assembly of the MST1–MOB1 complex to promote YAP activity in PC. Importantly, the MST4–MOB4 complex is up-regulated in PC and negatively associated with patient survival. Hence the MST4–MOB4 complex represents a new regulator of the Hippo–YAP pathway that coevolved with the MST1–MOB1 complex.

Results

MST4 directly interacts with MOB4

Given the phylogenetic classification of MST kinases and the fact that MST1/2 kinases form a complex with MOB1 in the Hippo–YAP pathway, we hypothesized that MST4 kinase may also utilize the MOB family of proteins as adaptor or partner. Because both MST4 and MOB4 have been identified as components of the STRIPAK complex, we reasoned that MST4 and MOB4 could form a complex analogous to the MST1/2–MOB1 complex. To test this possibility, we first performed coimmunoprecipitation (co-IP) assay in HEK293FT cells overexpressing MST4 and MOB4. FLAG-tagged MST4 can readily pull down HA-tagged MOB4 (Fig. 1*B*). Moreover, endogenous MST4 is also associated with endogenous MOB4 (Fig. 1*C*). Next, we examined the cellular localization of MST4 and MOB4. Our confocal microscopy experiment detected a significant signal for colocalization of MST4 and MOB4 in PANC-1 cells (Fig. 1*D*). Together, these results indicate that MST4 indeed physically interacts with MOB4 in cells.

To further characterize the interaction between MST4 and MOB4, we overexpressed and purified the proteins of MST4 and MOB4 in *Escherichia coli*. Pulldown assay using the purified proteins showed that MBP-tagged MST4, but not the MBP control, can directly interact with MOB4 (Fig. 1*E*). Consistent with this observation, gel-filtration chromatography revealed that MST4 and MOB4 are coeluted in a single peak with a fixed molar ratio (Fig. 1*F* and Fig. S1). Furthermore, bio-layer interferometry (BLI) experiment detected a dose-dependent binding between MST4 and MOB4 with a dissociation constant (K_d) of 1.67 μM (Fig. 1*G*). Taken together, these results indicate that MST4 directly binds MOB4 to form a stable complex.

MST4 auto-phosphorylation at Thr-327/328 is critical for binding MOB4

Because MOB1 is known to bind MST1/2 kinases in a phosphorylation-dependent manner (8), we then asked whether assembly of the MST4–MOB4 complex is also dependent on phosphorylation. To this end, we performed an *in vitro* pulldown assay using purified recombinant proteins of MST4 and MOB4. MST4 can directly bind to either of the two MOB4 isoforms although treatment with λ protein phosphatase (λPP) markedly reduced such interaction (Fig. 2*A*). However, incubation of MST4 with ATP and $MgCl_2$ did not significantly affect its interaction with MOB4 (Fig. 2*A*), suggesting that the recombinant MST4 kinase is already autophosphorylated. Consistent with this notion, treatment with λPP but not ATP clearly shifted the electrophoretic band of MST4 toward the direction of lower molecular weight (Fig. 2*A*). To further verify the importance of MST4 auto-phosphorylation in binding MOB4, we treated MBP–MST4 with λPP, followed by treating the dephosphorylated MBP–MST4 with ATP. As shown in Fig. S2*A*, λPP-treated MST4 did not bind MOB4 but recovered the ability to bind MOB4 after treatment with ATP to induce auto-phosphorylation. Moreover, the kinase-inactive form of MST4 (MST4–K53R) was not able to bind MOB4 (Fig. S2*B*). Together, these results indicate that MST4 interacts with MOB4 in a phosphorylation-dependent manner, a feature previously observed for the assembly of the MST1/2–MOB1 complex.

To identify the specific region and site(s) of MST4 important for binding MOB4, we created a series of MBP-fused truncation mutants of MST4 and subjected the purified proteins to phosphorylation by WT MST4. Pulldown assay using these proteins revealed an essential role of the MST4 linker region for binding MOB4 (Figs. 1*A* and 2*B*). We then generated a group of MBP-fused MST4 linker proteins and phosphorylated them with untagged WT MST4. Subsequent pulldown assay showed that amino acids 316–335 of MST4 is the minimal region for binding MOB4 (Fig. 2*C*). Sequence analysis of MST4 revealed that

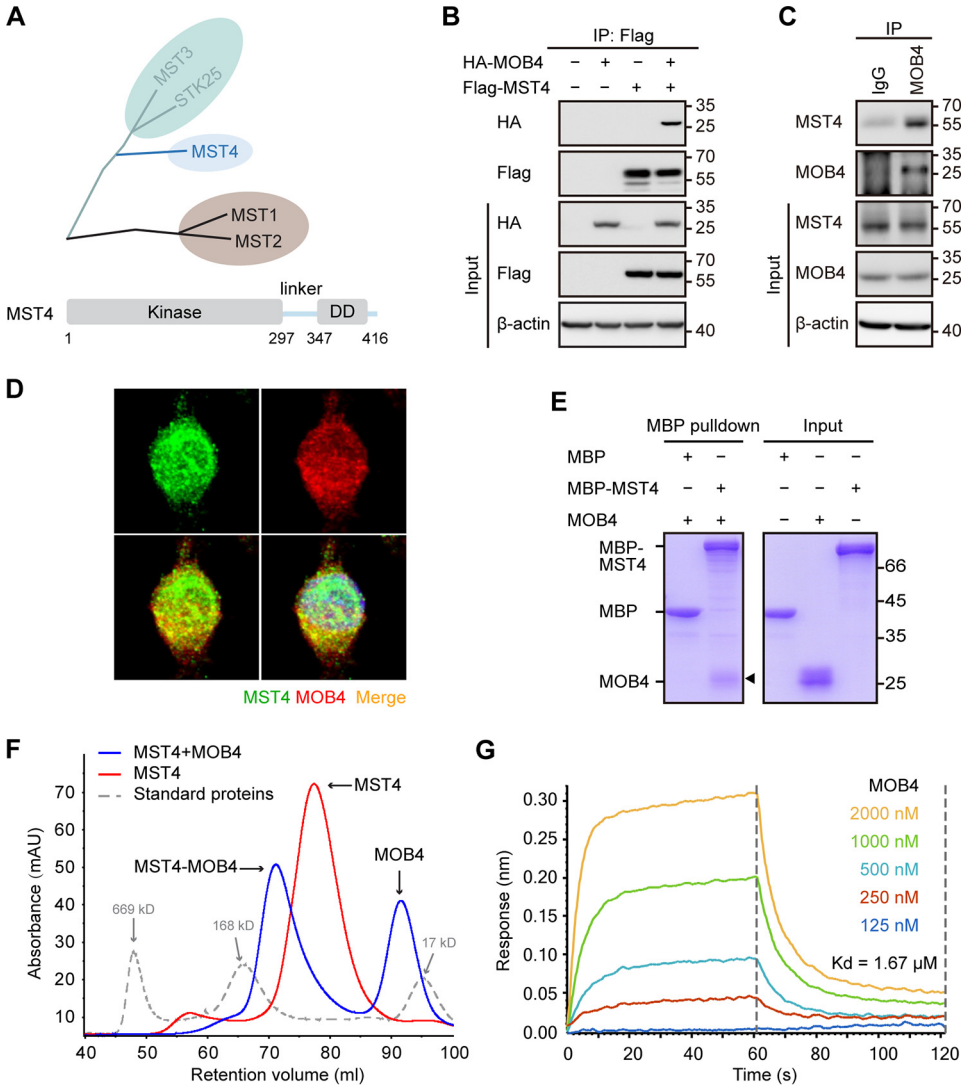

Figure 1. MOB4 directly binds to MST4. *A,* phylogenetic relationships within human MST protein kinase family (*top*) and schematic representation of domain organization of MST4. *Kinase,* kinase domain; *DD,* dimerization domain. *B* and *C,* coimmunoprecipitation and immunoblot analysis of exogenous (*B*) and endogenous (*C*) MST4 and MOB4 in HEK293FT cells. *IP,* immunoprecipitation. *D,* confocal microscope analysis of endogenous MST4 and MOB4 in PANC-1 cells. *E,* MBP pulldown analysis between MST4 and MOB4. The input and output samples were loaded on SDS-PAGE followed by CBB staining. *F,* UV traces of molecular weight standards (*dashed line*), MST4 (*red line*), or MST4 and MOB4 mixed at a 1:2 molar ratio (*blue line*) fractionated on a HiLoad 16/60 Superdex 200 pg gel filtration column. *G,* bio-layer interferometry analysis of the interactions of MST4 with various concentrations of purified MOB4 proteins. See also Fig. S1.

only four serine/threonine residues (possible auto-phosphorylation sites) exist in this region, *i.e.* Thr-320, Ser-325, Thr-327, and Thr-328. Next, we substituted each of these four amino acids with an alanine, and we measured their interactions with MOB4. Pulldown assay using purified proteins showed that none of the single mutations could abolish the binding of MST4 with MOB4 (Fig. S2*C*), indicative of multiple sites involved in the interaction.

Subsequently, we made a four-point mutation T320A/S325A/T327A/T328A (4A) and a three-point mutation S325A/T327A/T328A (3A) of MST4. As shown by the pulldown assay, either 4A or 3A mutation disabled the interaction of MST4 with MOB4 (Fig. S2*D*), suggesting that residues among Ser-325, Thr-327, and Thr-328 are essential for MOB4 binding. Further detailed mutational analysis targeting these three amino acids identified Thr-327 and Thr-328 of MST4 as the primary phosphorylation sites critical for binding MOB4 (Fig. 2*D*). Therefore, we synthesized a phospho-Thr-327/Thr-328 MST4 linker peptide (amino acids 320–335, "THPEWSFpTpTVRKKPDP") for further study. Isothermal titration calorimetry (ITC) confirmed that the phosphopeptide could readily bind to MOB4 with a dissociation constant (K_d) of 22.9 μM (Fig. 2*E*). Taken together, these results indicate that upon auto-phosphorylation at Thr-327 and Thr-328, the linker region of MST4 binds to MOB4.

MST4–MOB4 complex structurally resembles the MST1/2–MOB1 complex

To understand at an atomic level the interaction between MST4 and MOB4, we determined to a 1.9-Å resolution the crystal structure of MOB4 (amino acids 53–210) in complex with the synthetic phospho-Thr-327/Thr-328 MST4 linker peptide (Table 1 and Fig. 3*A*). The electron density is well defined for most residues of MOB4 (except its N-terminal 14 residues and residues 139–153) and the MST4 peptide (residues 324–333) (Fig. S3). There is one MOB4 molecule and one

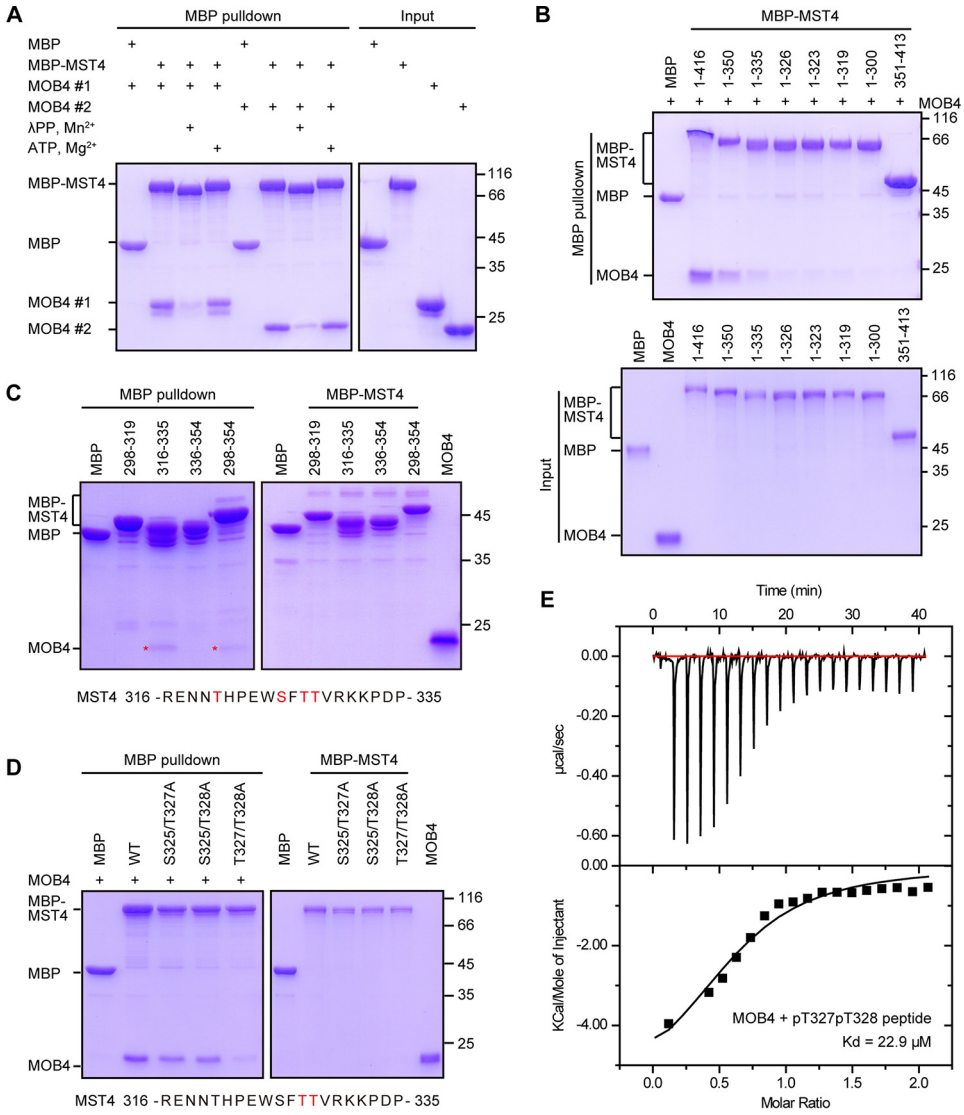

Figure 2. MST4 auto-phosphorylation at Thr-327/328 is critical for binding MOB4. *A,* pulldown analysis between MST4/pMST4 and MOB4. Purified protein of MBP-tagged MST4 was first dephosphorylated by λPP or further autophosphorylated. The input and output samples were loaded on SDS-PAGE followed by CBB staining. *MOB4 #1*, isoform 1 of MOB4; *MOB4 #2*, isoform 2 of MOB4, corresponding to amino acids 33–225 of isoform 1. *B–D*, pulldown analysis-based mapping of MOB4-binding region (*B* and *C*) and sites (*D*) on MST4. All MBP-tagged MST4 truncations and mutants were *in vitro* phosphorylated before use. The input and output samples were loaded on SDS-PAGE followed by CBB staining. *E,* ITC curves of the binding between MOB4 and the pMST4 (*pT327pT328*) peptide. Note: MOB4 protein used in *B–E* is isoform 2. See also Fig. S2.

pMST4 peptide in each asymmetric unit of the crystal, burying a total molecular interface of 550.9 Å^2. Moreover, the MOB4 molecule not only interacts with the MTS4 peptide in the same asymmetric unit, but it also contacts a symmetry-related MST4 peptide (Fig. 3*A*). Although this second interface is smaller (261.9 Å^2), it is likely for MST4 and MOB4 to form a 2:2 heterotetramer under physiological conditions given that the C-terminal domain of MST4 forms a homodimer (Fig. 1*A*).

The overall structure of the MST4–MOB4 complex resembles the previously determined MST2–MOB1 structure (PDB code 5BRM) (8, 38). In both cases, the phosphorylated MST peptides formed an intermolecular anti-parallel β-sheet with the L1 loop of MOBs (site 1), despite the lack of hydrophobic packing (site 2) in the MST4–MOB4 complex (Fig. 3, *B* and *C,* and Fig. S4*A*). The structure of MOB4 consists of six helices (α1–5 and η1) and a long loop region (L1) between helices α1 and α2, which folds into a four-helical bundle similar to MOB1 (Fig. 3*A* and Fig. S4, *B* and *C*)(8, 38). The conserved zinc ion (Zn1) is coordinated by the side chains of residues Cys-92, Cys-97, His-169, and His-174 (Fig. 3*C* and Fig. S4*C*). When compared with MOB1, however, MOB4 contains an additional zinc ion (Zn2), which is coordinated by the side chains of residues Cys-110, His-113, Cys-119, and His-127 (Fig. 3*C*).

At the phosphorylation site, the interactions between MSTs and MOBs are mainly mediated by salt bridges between the phosphate groups on the phosphorylated MST linker region and the basic amino acids on MOBs (Fig. 3, *D–F,* and Fig. S4*A*). In the MST4–MOB4 complex, phosphorylated Thr-328 and Thr-327 of MST4 form several ion pairs and hydrogen bonds with a cluster of positively charged residues Arg-161, Arg-162, and Arg-165 of MOB4, explaining the phosphorylation-dependent nature of the complex assembly (Fig. 3, *D* and *E*). Corresponding to pThr-328 of MST4, pThr-378 of MST2 similarly

Table 1
Data collection and refinement statistics
Statistics for the highest-resolution shell are shown in parentheses.

	MST4-MOB4
Data collection	
Wavelength (Å)	0.9785
Space group	*C* 1 2 1
Cell dimensions	
a, *b*, *c* (Å)	88.5, 34.0, 61.0
α, β, γ (°)	90.0, 122.7, 90.0
Resolution (Å)	50.00–1.90 (1.93–1.90)
No. of reflections	77,777
R_{merge}	0.109 (0.798)
$I/\sigma(I)$	15.5 (2.5)
Completeness (%)	98.9 (99.0)
Redundancy	6.4 (5.5)
Wilson *B*-factor (Å^2)	18.9
Refinement	
Resolution (Å)	29.59–1.90 (1.93–1.90)
R_{work}/R_{free}	0.1527/0.1977
No. of atoms	
Protein	1138
Zinc ion	2
Water	75
Average *B* factor (Å)	32.99
Root mean square deviations	
Bond length (Å)	0.016
Bond angles (°)	1.350
Ramachandran	
Favored (%)	96
Allowed (%)	4
Outliers (%)	0

contacts a patch of positively charged residues Lys-153, Arg-154, and Arg-157 of MOB1 (Fig. 3*F* and Fig. S4*A*). Moreover, sequence analysis revealed that the interface residues of the MST4–MOB4 complex are evolutionarily conserved (Fig. S4*D*).

Notably, the assembly of the MST4–MOB4 complex requires two phosphorylated threonines (Thr-327 and Thr-328). In a dimeric context, one molecule of MST4 interacts via pThr-327 and pThr-328, respectively, with two copies of MOB4 (Fig. 3*D*), whereas the arginine cluster of each MOB4 molecule binds pThr-327 from one MST4 and pThr-328 from the other (Fig. 3*E*). Interestingly, MST2 also contains multiple phospho-Thr-Met motifs in the linker region, including Thr-349, Thr-356, and Thr-364, which function redundantly for MOB1 binding (8). Thus, it appears that homodimerized MST kinases could use multiple phosphorylation sites to efficiently recruit MOB proteins. Taken together, these results demonstrate the structural similarity between the MST4–MOB4 and MST1/2–MOB1 complexes, raising the possibility of promiscuous pairing between MSTs and MOBs.

Key interface residues determine alternative pairing of MSTs with MOBs

To verify our structural analysis and define key residues for MST4 interaction with MOB4, we performed mutational analysis. Substitution of any single interface residues of MST4 with alanine (S325A, F326A, T327A, T328A, V329A, and R330A) mildly reduced the binding of MOB4, whereas a combined mutation of T327A and T328A (2TA) abolished its interaction with MOB4 (Fig. 4*A* and Fig. S5*A*). Mutations W106A, I107A, and L109A of MOB4 decreased its association with MST4, whereas mutations R161A, R162A, R165A, and R161A/R162A/R165A (3RA) abolished the complex assembly (Fig. 4*B* and Fig. S5*B*). Further BLI analyses also revealed residues Thr-327/328 of MST4 and Arg-161/162/165 of MOB4 as the most critical interface residues (Fig. 4, *C–F,* and Fig. S5, *C* and *D*). The co-IP experiments further confirmed in cells the importance of these interface residues (Fig. 4, *G* and *H*).

With these key interface residues in mind, we analyzed the amino acid sequences of MSTs and MOBs based on available structure information (Fig. S5*E*), attempting to find the preferential pairing between MSTs and MOBs. As described earlier, MST1/2 kinases have multiple phosphorylation sites corresponding to Thr-327 and Thr-328 of MST4. However, MST3 only contains one threonine (Thr-340) with an adjacent residue being Glu-343 in the region corresponding to Thr-327/328 of MST4, which is disadvantageous to form hydrophobic interaction and cation-π bond with MOB4 (Fig. S5*E*). Similarly, the two critical threonines are replaced by prolines (Pro-322 and Pro-323) in STK25, making it unlikely to bind MOB4. Meanwhile, residues Arg-161/162/165 in MOB4 are highly conserved in MOB1 but not in other MOBs. These observations hint at alternative pairing between MSTs and MOBs, *i.e.* MST4 could pair with either MOB4 or MOB1, and MOB4 could pair with either MST4 or MST1/2. To verify this possibility, we performed pulldown assays using purified recombinant proteins of MSTs, including MST1, MST2, MST3, MST4, and STK25, and MOBs, including MOB1A, MOB2, MOB3A, and MOB4. Indeed, MST4 cannot only bind to MOB4 but can also readily interact with MOB1 (Fig. 4*I* and Fig. S5*F*). In addition to MST4, MOB4 can also bind MST1 to a certain extent (Fig. 4*J* and Fig. S5*G*). Taken together, these results define Thr-327/328 of MST4 and Arg-161/162/165 of MOB4 as primary sites for complex assembly, which confers alternative pairing of MST4 with MOB4 or MOB1 and that of MOB4 with MST4 or MST1.

MST4–MOB4 and YAP are up-regulated but MST1 is down-regulated in PC

Previously the MST1 kinase has been implicated in pancreatic cancer (24). To further characterize the biological functions of MST–MOB complexes in a context of tumorigenesis, we assessed the clinical significance of the MST4–MOB4 complex in PC. Analysis of the microarray datasets publicly available revealed that the mRNA levels of both *MST4* and *MOB4* are significantly up-regulated in the clinical specimens of patients with PC (Fig. 5*A* and Fig. S6*A*). Moreover, the mRNA levels of *MST4* positively correlate with that of *MOB4* in PC patients (Fig. 5*B* and Fig. S6*B*). Furthermore, elevated expression levels of *MST4* and *MOB4* negatively correlate with the survival rates of PC patients (Fig. 5*C* and Fig. S6, *C* and *D*).

Similar to *MST4* and *MOB4*, the expression of *YAP*, as well as its target genes *BIRC5* and *BCL2L1*, is also up-regulated in PC (Fig. 5*D*). Moreover, the mRNA levels of *MST4* and *MOB4* positively correlate with those of *YAP* in PC (Fig. 5*E*). Consistent with these observations, our immunohistochemical (IHC) analysis revealed that the positive rates of MST4 and MOB4 in PC samples are significantly higher when compared with those of the healthy ones (Fig. 5*F*). Meanwhile, the expression of YAP is also highly increased in PC, although the staining of MST1 is

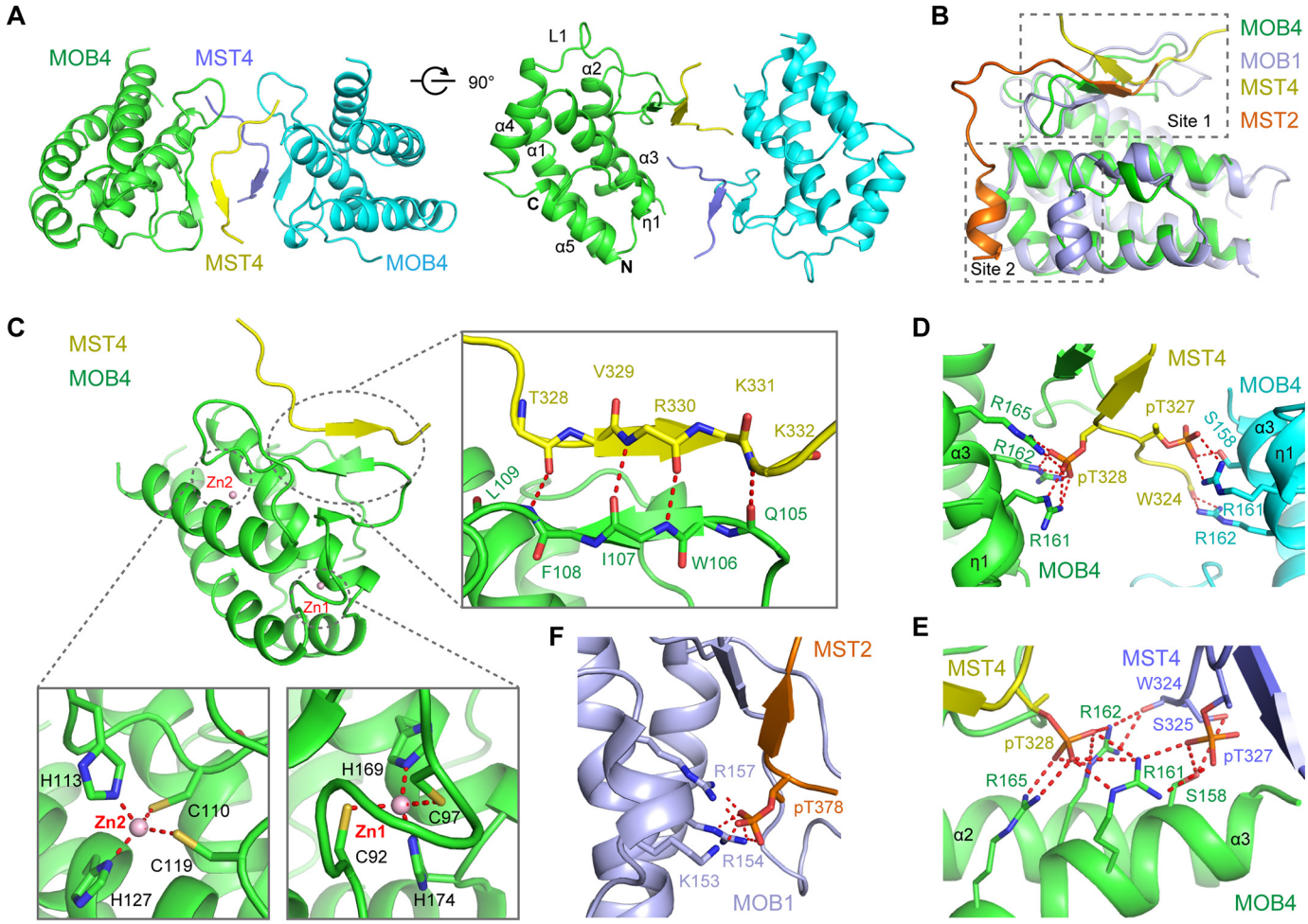

Figure 3. Crystal structure of the MST4–MOB4 complex. *A,* cartoon views of two structurally symmetrical MOB4s in complex with the phosphorylated MST4 peptide. The core MOB4 molecules are colored *green* and *cyan*, and the MST4 peptides are colored *yellow* and *slate*, respectively. *B,* overall structural comparison of pMST4–MOB4 with pMST2–MOB1 complex (PDB 5BRM). The core MOB4 (*green*) was superimposed with MOB1 (*light blue*). The pMST4 peptide is colored *yellow*, and the pMST2 peptide is colored *orange*. The common interface (site 1) and the unique interface contained in pMST2–MOB1 (site 2) are indicated. *C,* zoomed-in views of the two zinc ions, Zn1 and Zn2, coordinated by MOB4 (*bottom*) and the β-sheet formed between MOB4 and MST4 (*right*). Hydrophobic interactions within the β-sheet are indicated. *D* and *E*, zoomed-in views of pMST4 and MOB4 interactions at the pThr-binding sites. *F,* zoomed-in views of pMST2 and MOB1 interactions at the pThr-binding site (corresponding to pThr-328 of MST4). Note: *red dashed lines* represent hydrogen bonds or electrostatic interactions. The interface residues are labeled and highlighted by a *stick* model. See also Figs. S3 and S4.

significantly decreased (Fig. 5*G*). Taken together, these results indicate that the MST4–MOB4 complex is up-regulated in PC and negatively correlated with patient survival.

MST4–MOB4 and MST1–MOB1 complexes have opposite functions in PC

Because MST4 and MST1 were found to be differentially expressed in PC, we suspected that MST4–MOB4 may play a role different from that of MST1–MOB1 in the regulation of tumor cell proliferation and migration. Thus, we examined the potential effect of the MST4–MOB4 and MST1–MOB1 complexes on the proliferation and migration of PANC-1 cells. Our MTT assay showed that knockdown of either MST4 or MOB4 with short hairpin RNA (shRNA) markedly decreased the proliferation of PANC-1 cells, although depletion of both MST4 and MOB4 almost blocked the cell growth (Fig. 6*A*). Meanwhile, transwell assay showed that knockdown of either MST4 or MOB4 reduced PANC-1 cell migration; knockdown of both MST4 and MOB4 elicited a stronger inhibitory effect (Fig. 6*B*). On the contrary, overexpression of either MST4 or MOB4 increased the proliferation of PANC-1 cells; coexpression of MST4 and MOB4 had an even larger promoting effect toward cell proliferation (Fig. 6*C*). However, the interface mutations (MST4–2TA and MOB4–3RA) disrupting the MST4–MOB4 complex abrogated its regulatory function (Fig. 6*C*). Similarly, overexpression of WT MST4 and/or MOB4, but not their 2TA and/or 3RA mutants, significantly enhanced the migration of PANC-1 cells (Fig. 6*D*). Together, these results indicate that MST4 and MOB4 cooperate with each other to promote the proliferation and migration of PANC-1 cells.

In contrast to the oncogenic role of the MST4–MOB4 complex, the MST1–MOB1 complex is expected to act as a tumor suppressor. Indeed, knockdown of MST1 and/or MOB1 significantly promoted the proliferation and migration of PANC-1 cells (Fig. 6, *E* and *F*); overexpression of WT MST1 and/or MOB1, but not their mutants disabled for the complex formation (8), inhibited cell proliferation and migration (Fig. 6, *G* and *H*). Taken together, these results indicate that the MST4–MOB4 and MST1–MOB1 complexes have opposite biological functions despite their structural similarity.

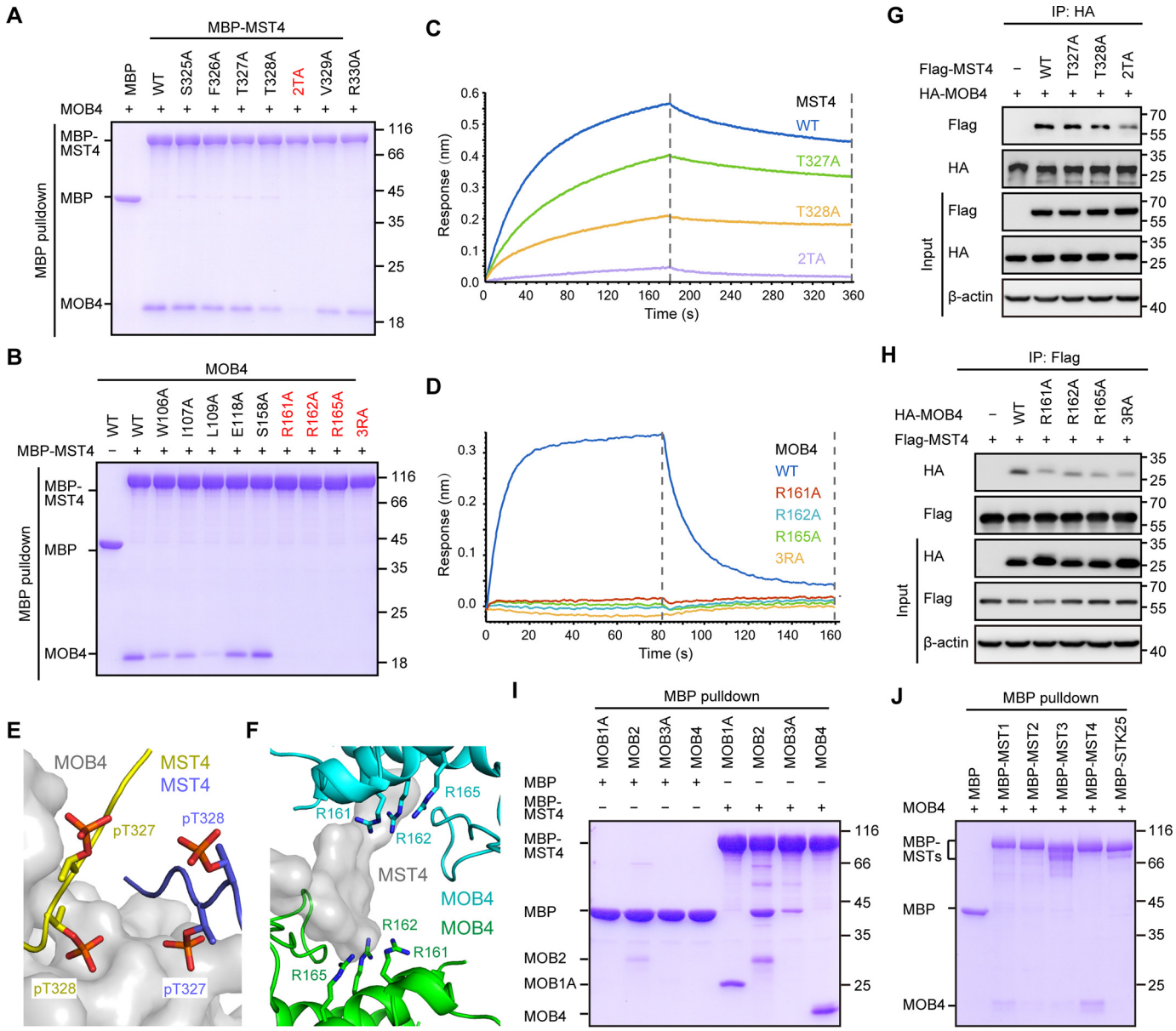

Figure 4. Key interface residues and alternative pairing of MST4 and MOB4. *A,* pulldown analysis between MOB4 and various MST4 mutants. *2TA,* T327A/T328A. *B,* pulldown analysis between MST4 and various MOB4 mutants. *3RA,* R161A/R162A/R165A. *C,* BLI analysis of interactions of WT or mutant MST4 with WT MOB4. *Colored curves* are the experimental traces of BLI experiments for mutations in MST4. *D,* BLI analysis of interactions of WT or mutant MOB4 with WT MST4. *Colored curves* are the experimental traces of BLI experiments for mutations in MOB4. *E* and *F,* critical residues in MST4 (*E*) or MOB4 (*F*) for MOB4 (*E*) or MST4 (*F*) binding. The molecules MOB4 in *E* and MST4 in *F* are shown by surface models and colored *gray*. *G* and *H,* coimmunoprecipitation and immunoblot analysis of the interactions between MOB4 (*G*) or MST4 (*H*) and key MST4 (*G*) or MOB4 (*H*) mutants in lysates of HEK293FT cells transfected with the indicated plasmids. *I* and *J,* pulldown analyses between MSTs and MOBs. The indicated proteins of MBP-tagged MST4 (*I*) or different MST proteins (*J*) were coupled on amylase resin and then mixed with different MOBs (*I*) or MOB4 (*J*), respectively. All MST proteins were *in vitro* autophosphorylated before use. The input and output samples were loaded on SDS-PAGE followed by CBB staining. The MOB4 protein used here is isoform 2. Note: MOB4 protein used in *A–D* is the fragment containing amino acids 53–210. See also Fig. S5.

MST4–MOB4 complex antagonizes the MST1–MOB1 complex in PC

Considering the importance of MST1 in the Hippo–YAP pathway and PC progression (39–41), we postulated that MST4 might have a functional interplay with MST1 and thus regulate YAP activity in PC. To test this possibility, we first examined the transcription of the YAP target gene *CTGF* in PANC-1 cells with MST1/MST4 knockdown. As expected, knockdown of MST1 relieved its inhibition of YAP and therefore resulted in elevated mRNA level of *CTGF*; and knockdown of MST4 significantly decreased the expression of *CTGF* when compared with the control group (Fig. 7*A*). Moreover, the mRNA levels of the Hippo–YAP target genes (*CTGF* and *BIRC5*) are significantly increased in PANC-1 cells overexpressing MST4 or MOB4; coexpression of MST4 and MOB4 further enhanced such an effect (Fig. 7*B*). However, the mutants of MST4 and MOB4 impaired for complex formation failed to promote the transcription of *CTGF* and *BIRC5* (Fig. 7*B*). These results suggest that the MST4–MOB4 complex indeed regulates the Hippo–YAP signaling.

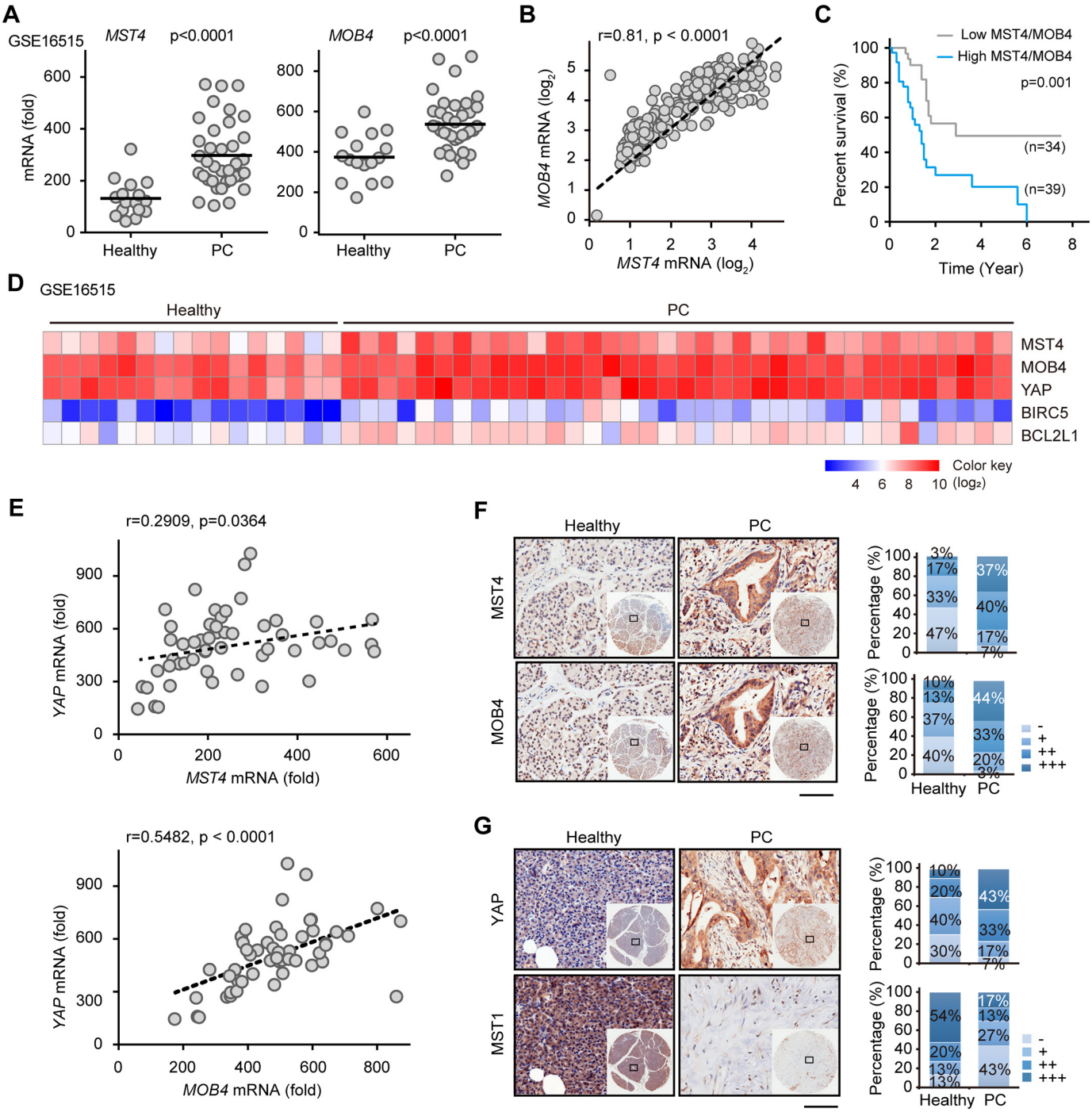

Figure 5. Clinical significance of MST4 and MOB4 in PC. *A, MST4* and *MOB4* mRNA levels in human healthy and PC tissue samples using previously published microarray database (GEO: GSE16515, $n = 52$). The *horizontal lines* in the scatter plot represent group medians. *p* values were determined by Student's *t* test. *B,* GEPIA (53) correlation analysis of *MST4* and *MOB4* mRNA levels in PC patients. Correlation was determined by Pearson's correlation based on the TCGA and GTEx datasets. *C,* survival curves of PC patients with high or low MST4/MOB4 expression based on the TCGA data. Grouped data obtained from http://www.proteinatlas.org/ (Please note that the JBC is not responsible for the long-term archiving and maintenance of this site or any other third party hosted site.) and survival curves were calculated using GraphPad Prism 7.0 according to the Kaplan-Meier method; survival analysis was performed using the log rank test. *D*, heat map for the expression levels of *MST4, MOB4,* and *YAP,* and YAP target genes *BIRC5* and *BCL2L1* in human healthy and PC tissue samples using previously published microarray database (GEO: GSE16515). *E,* correlation analysis between *YAP* and *MST4* or *MOB4* in patients with PC was determined by Pearson's correlation based on the previously published microarray database (GEO: GSE16515). *F,* representative images of MST4 and MOB4 protein levels in human PC and their paired adjacent healthy tissues by IHC experiments. *Scale bars*, 20 μm. MST4 and MOB4 staining levels in healthy and PC tissues are indicated as negative (−), weak (+), moderate (++), and strong (+++), respectively. *G,* representative images of YAP and MST1 protein levels in human PC and their paired adjacent healthy tissues by IHC experiments. *Scale bars*, 20 μm. YAP and MST1 staining levels in healthy and PC tissues are indicated as negative (−), weak (+), moderate (++), and strong (+++), respectively. See also Fig. S6.

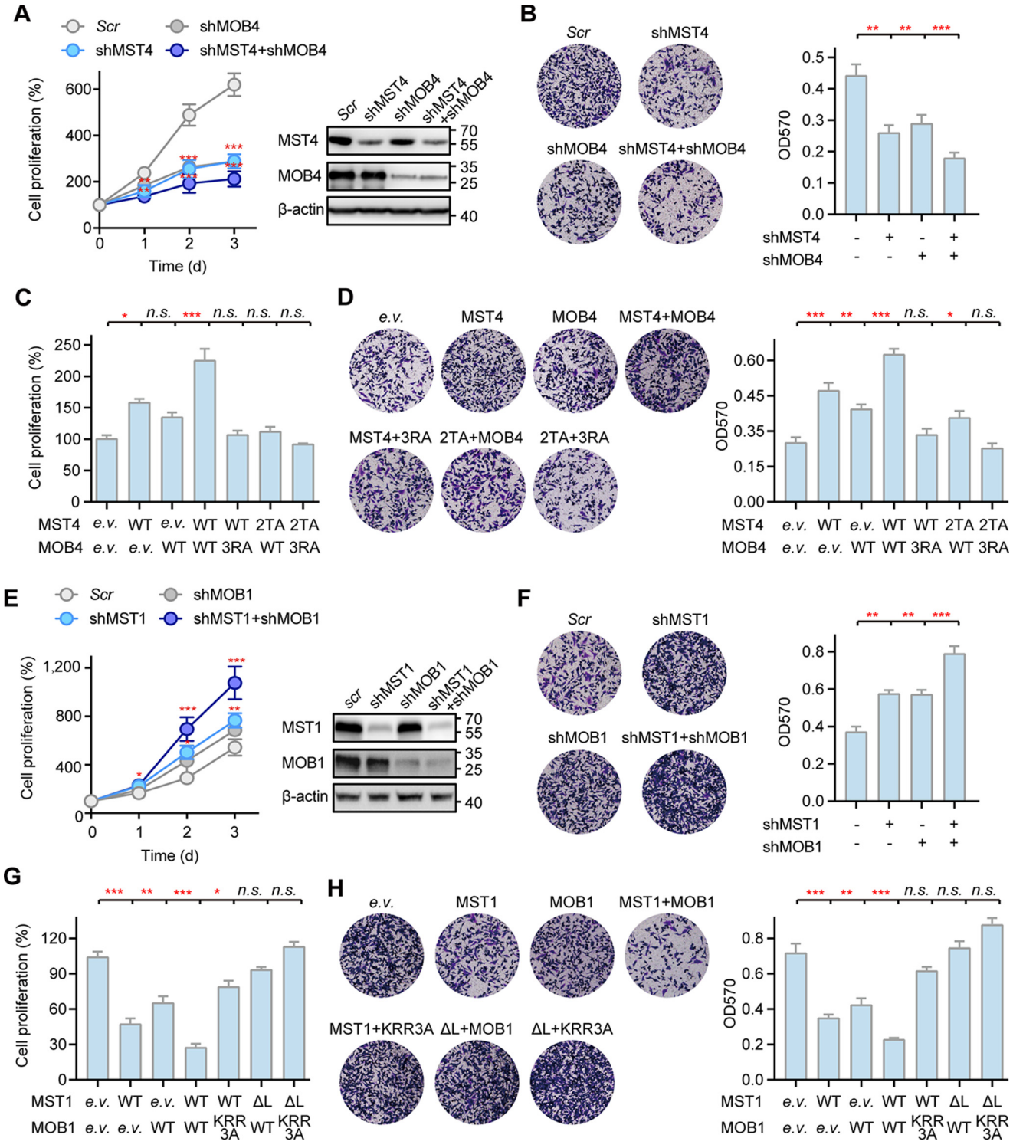

Figure 6. Opposite functions of the MST4–MOB4 and MST1–MOB1 complexes. *A,* cell proliferation rate of PANC-1 cells infected with lentivirus-mediated shRNAs, including scramble (*Scr*), shMST4, and shMOB4. *B,* cell migration of PANC-1 cells transfected with the indicated shRNAs. *C* and *D,* cell growth and cell migration of PANC-1 cells after lentivirus-mediated overexpression of the indicated proteins. *E* and *F,* cell proliferation rate and cell migration of PANC-1 cells transfected with the indicated shRNAs. *G* and *H,* cell growth and cell migration of PANC-1 cells after lentivirus-mediated overexpression of the indicated proteins. Δ*L,* linker deletion; *KRR3A,* K153A/R154A/R157A. Note: cell proliferation and migration was determined by MTT and Transwell migration assay, respectively. *Bar graphs* represent the means ± S.D. Experiments we repeated three times. Unpaired *t* tests were used to compare the difference between two groups. *, significant relative to control, $p < 0.05$; **, $p < 0.01$; ***, $p < 0.001$. *n.s.*, no statistical significance.

Given the structural similarity of the MST–MOB complexes and the alternative pairing of MST4–MOB4/MOB1 and MOB4–MST4/MST1 (Fig. 4, *I* and *J*), we reasoned that the MST4–MOB4 complex might dynamically assemble and disassemble to interfere the MST1–MOB1 complex, leading to YAP activation (Fig. 7*C*, *model*). To test this hypothesis, we assessed the potential effect of MST4 and MOB4 on the interaction between MST1 and MOB1. Our IP assay showed that

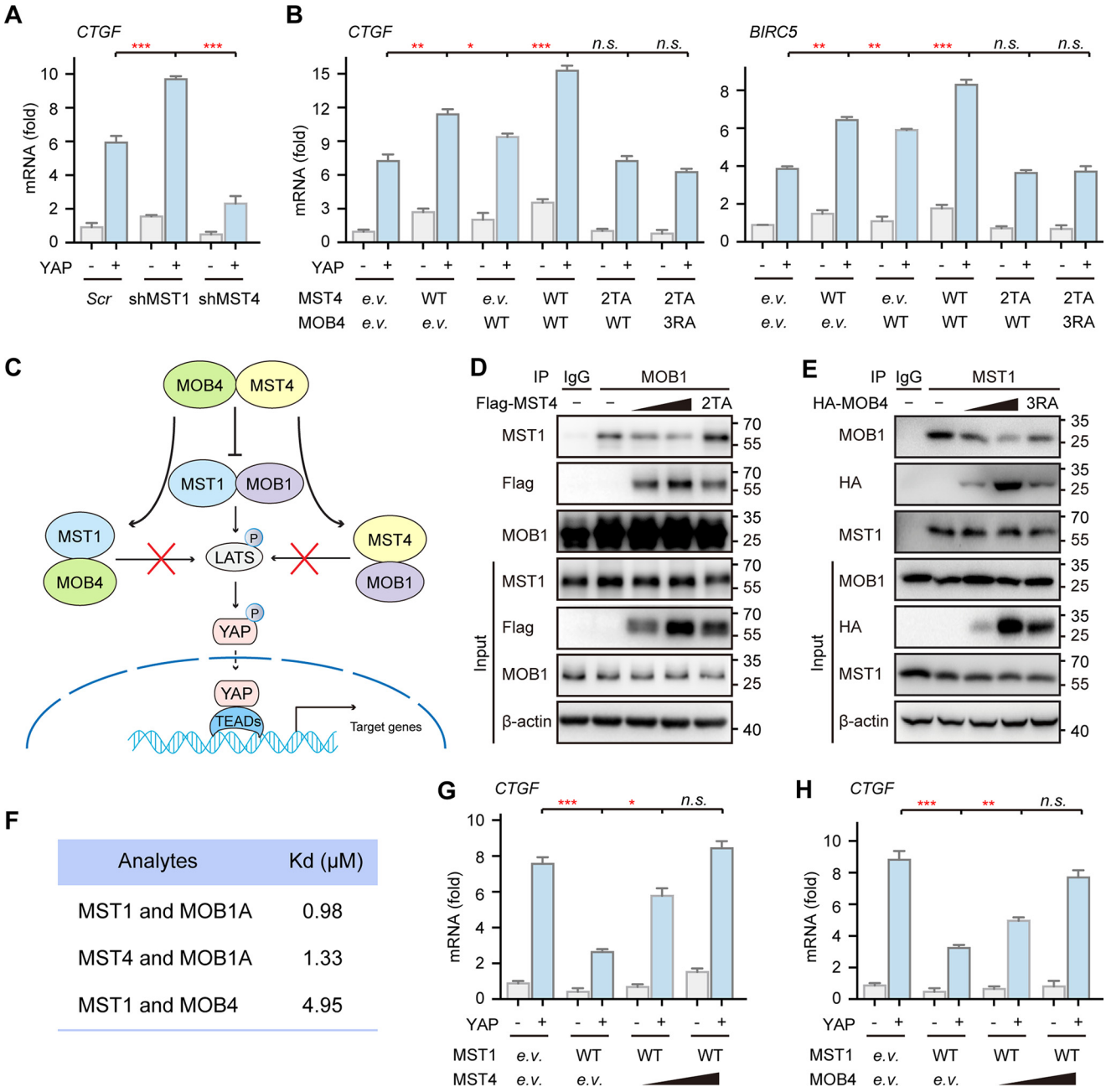

Figure 7. MST4 and MOB4 disturb the MST1–MOB1 complex to activate YAP. *A,* transcription of YAP target gene *CTGF* in PANC-1 cells infected with lentivirus-mediated shRNAs, including scramble (*Scr*), shMST1, and shMST4, as evaluated by real time PCR (RT-PCR). *B,* transcription of YAP target genes *CTGF* and *BIRC5* in PANC-1 cells infected with lentivirus-mediated expression of the indicated plasmids, as evaluated by RT-PCR. *C,* proposed model for MST4–MOB4-mediated YAP activation. *D,* competitive binding of MST1/4 to MOB1 in PANC-1 cells. *E,* competitive binding of MOB1/4 to MST1 in PANC-1 cells. *F,* dissociation constants (K_d) between the indicated analytes, as evaluated by BLI experiments. *G* and *H,* effect of MST4 (*G*) or MOB4 (*H*) on MST1-mediated YAP target gene inhibition in PANC-1 cells, as evaluated by RT-PCR. Note: *bar graphs* represent the means ± S.D. Experiments were repeated three times. Unpaired *t* tests were used to compare the difference between two groups. *, significant relative to control, $p < 0.05$; **, $p < 0.01$; ***, $p < 0.001$. *n.s.*, no statistics significance. See also Fig. S7.

WT MST4, but not its mutant disabled for complex formation, dose-dependently inhibits the binding of MST1 with MOB1 (Fig. 7*D*). Similarly, expression of WT MOB4, but not its mutant, also impairs the interaction between MST1 and MOB1 (Fig. 7*E*). Moreover, *in vitro* BLI experiments revealed the binding affinity between MST4 and MOB1A, as well as the affinity between MST1 and MOB4 to be comparable with that between MST1 and MOB1A (Fig. 7*F* and Fig. S7). Interestingly, the kinetics of the MST–MOB binding analyses indicated MOB4 associated and dissociated with MST1/4 kinases with a much higher rate (quicker) than did MOB1 with these kinases. Considering their increased abundances in PC, MST4 and MOB4 may readily disrupt the association between MST1 and MOB1 in tumor cells. Consistent with these observations, overexpression of MST4 or MOB4 rescues, in a dose-dependent manner, MST1-mediated inhibition of YAP-induced target genes' transcription (Fig. 7, *G* and *H*). Taken together, these results indicate that the MST4–MOB4 complex can disturb

the assembly of the MST1–MOB1 complex, promoting YAP activity in PC.

Discussion

As the upstream core of the Hippo–YAP signaling pathway, MST1/2 kinases in complex with MOB1 suppress multiple cancer progression by inhibiting the activity of YAP (7, 8, 42–45). Here, we identified an MST4–MOB4 complex structurally analogous to the MST1/2–MOB1 complex. Despite their structural similarities, the MST4–MOB4 complex exerts an oncogenic role in PC, whereas the MST1–MOB1 complex shows a tumor suppressor effect. Up-regulated in PC, the MST4–MOB4 complex can interfere with the assembly of the MST1–MOB1 complex, and therefore relieve its inhibition of YAP.

The interaction between MST4 and MOB4 depends on the auto-phosphorylation of MST4 Thr-327 and Thr-328. Previously, a peptide library screening identified the optimal MOB1-binding sequence, which displayed a preference for hydrophobic residues in the +1 position and hydrophobic or basic residues in the +2 to +4 positions (46). The sequence of MST4 for MOB4 binding also matches this feature, which together with our structural and biochemical studies indicate a conserved assembly pattern between the MST and MOB proteins. Thus, the MST4–MOB4 and MST1–MOB1 complexes are likely evolved from the same origin with conserved structural assembly but divergent biological functions. In other words, the evolutionarily conserved MSTs–MOBs assembly can function differently or even in opposite directions.

Because of the structural similarity and conservation of key interface residues, MST4 can alternatively pair with either MOB4 or MOB1, and so can MOB4 with either MST4 or MST1. For example, structural and sequence analyses revealed that the three basic residues Arg-161, Arg-162, and Arg-165 of MOB4 critical for binding MST4 are highly conserved in MOB1 (Lys-153, Arg-154, and Arg-157). Therefore, MOB1 may utilize a similar manner to interact with MST4, although MOB4 could also bind to MST1 in a similar fashion. In contrast to the tumor suppressor effect of the MST1–MOB1 complex, the MST4–MOB4 complex promotes the proliferation and migration of PANC-1 cells. Moreover, expressions of both MST4 and MOB4 are significantly increased in PC and negatively correlated with patient survival, whereas MST1 is significantly down-regulated. In such context, the excessive MST4 and MOB4 can disturb the MST1–MOB1 complex by competitively pairing with MST1/MOB1. Consistent with this notion, MOB3A/B/C was reported to negatively regulate MST1 in glioblastoma multiforme cells through direct MOB3A/B/C-MST1 tethering (16).

The MST4 kinase may promote cell growth and modulate multiple cancer progression, yet the behind mechanisms is unclear (11, 23, 27, 28). At this stage, it remains to be addressed whether the MST4–MOB4 and MST1–MOB1 complexes have similar interplay in cancers other than PC. Moreover, besides MOB1 and MOB4, MST4 can also bind to MOB2 to a certain extent. In addition to MOB1, the MST1 kinase also binds MOB3A/B/C (8, 16). Thus, the selective pairing of MSTs–MOBs and their specific functions are perplexing and could be context-dependent. In this regard, the potential interplay among different MSTs and MOBs clearly warrants further investigation.

In summary, this work identified an MST4–MOB4 complex that structurally resembles but functionally antagonizes the MST1–MOB1 complex to positively regulate YAP activity. The divergent evolution of MST–MOB complexes highlights the intricate yet balanced regulation of the Hippo–YAP signaling.

Experimental procedures

Plasmids and antibodies

Full-length or truncated human MOB1A, MOB3A, and MOB4 were cloned into a modified pET-28a vector that includes an N-terminal tobacco etch virus (TEV) protease-cleavable His_6–SUMO tag. The coding region of MST1, MST2, MST3, MST4, STK25, and MOB2 was cloned into another modified pET-28a vector that includes an N-terminal TEV protease-cleavable maltose-binding protein (MBP) tag. For mammalian expression vectors, FLAG–MST4 has been described previously (12); HA–MOB1A was a kind gift from Professor Lei Zhang (Shanghai Institute of Biochemistry and Cell Biology, Shanghai, China). MST1 and YAP were cloned into pCDNA-3.1–3*FLAG vector, and MOB4 was cloned into pCDNA-3.0-HA vector. All lentivirus-mediated knockdown plasmids were constructed in a modified pLKO.1 vector. For lentivirus-mediated overexpression, MST1, MST4, MOB1A, and MOB4 were constructed into a pCDH1-MCS-CoGFP vector. All mutants were generated by site-directed mutagenesis. All constructs were verified by DNA sequencing.

Antibody specific for human MST4 was produced by Shanghai Immune Biotech Co., Ltd., and has been described previously (36). Antibody to FLAG (F3165) was from Sigma. Antibody to HA (rabbit, catalog no. 3724), MOB1 (catalog no. 13730), and MST1 (rabbit, catalog no. 3682, used in immunoblot analysis) was from Cell Signaling Technology. Antibody to MOB4 (sc-165980), HA (mouse, sc-7392), and MST1 (mouse, sc-515051, used for immunoprecipitation), and YAP (sc-271134) was from Santa Cruz Biotechnology. Goat anti-rabbit secondary antibody (catalog no. 31460) and goat anti-mouse secondary antibody (catalog no. 31430) were from ThermoFisher Scientific.

Cells

HEK293FT cells was obtained from Shanghai Life Academy of Sciences cell library (Shanghai, China), and PANC-1 cells were the kind gift from Professor Mofang Liu (Shanghai Institute of Biochemistry and Cell Biology, Shanghai, China) (47). All cells were maintained in DMEM supplemented with 10% heat-inactivated fetal bovine serum (FBS), 100 μg/ml penicillin, and 100 μg/ml streptomycin at 37 °C with 5% CO_2 in a humidified incubator (ThermoFisher Scientific, Waltham, MA).

Protein expression and purification

All prokaryotic constructs were expressed in *E. coli* BL21 (DE3) CodonPlus cells by the induction of 0.5 mM isopropyl β-D-thiogalactopyranoside in Terrific Broth medium at 16 °C. For MOB4 proteins, cells were harvested by centrifugation 16 h post-induction and then resuspended with lysis buffer (20 mM

HEPES, pH 7.5, 500 mM NaCl, 5% glycerol, 1 mM DTT, and 20 mM imidazole) before being lysed. The cell debris was removed by centrifugation at 18,000 rpm for 40 min at 4 °C, and the soluble fraction was loaded onto nickel-Sepharose pre-equilibrated with lysis buffer. After washing with lysis buffer containing 20 and 40 mM imidazole, proteins were eluted with lysis buffer supplemented with 400 mM imidazole and then digested by TEV protease to remove the N-terminal His_6–SUMO tag. The target proteins were further purified by gel-filtration chromatography (HiLoad 16/60 Superdex 75, GE Healthcare) in buffer containing 20 mM HEPES, pH 7.5, 200 mM NaCl, and 1 mM DTT.

Human MOB1A and MOB3A proteins were purified following the same procedure as MOB4. The MBP-tagged proteins were purified by amylase resin and size-exclusion chromatography (HiLoad 16/60 Superdex 200, GE Healthcare).

Crystallization, structural determination, and refinement

For crystallization, the purified full-length or truncated MOB4 proteins were respectively concentrated to 10 mg/ml and then mixed with the phospho-MST4 peptide (pMST4, "THPEWSFpTpTVRKKPDP") at a 1:4 molar ratio to obtain the pMST4–MOB4 complexes. Of all constructs tried, the pMST4–MOB4(53–210) complex crystallized readily. Crystals were grown at 16 °C using the sitting-drop vapor diffusion method in a reservoir solution consisting of 0.1 M HEPES, pH 7.5, 30% PEG 1000. The crystals were cryo-protected with the reservoir solution supplemented with 30% glycerol and flash-cooled in liquid nitrogen before data collection. Diffraction data were collected at beamline BL19U1, Shanghai Synchrotron Radiation Facility (SSRF) of China, and processed using HKL3000 (48). The structure was solved by the single-wavelength anomalous diffraction method using the anomalous signal from zinc. Automated model building was performed with CCP4 i2, and the structure was refined using phenix.refine and Coot (49–52).

MBP pulldown assay

To obtain MBP-pMST4, purified MBP–MST4 was autophosphorylated at 30 °C for 30 min in the presence of 1 mM ATP, 5 mM $MgCl_2$. To dephosphorylated MBP-MST4, purified MBP–MST4 was treated with λPP with a mass ratio of 1:100 at 30 °C for 30 min in the presence of 10 mM $MnCl_2$. The MBP-fused linker fragments of MST4 were phosphorylated by untagged full-length MST4 and repurified with amylase resin to remove untagged MST4. MBP-fused MST1, MST2, MST3, and STK25 were phosphorylated or dephosphorylated following the same procedures as MST4.

For pulldown assays, MBP-fused proteins coupled on amylase resin were mixed with different prey proteins at 4 °C for 1 h in the buffer containing 20 mM HEPES, pH 7.5, 100 mM NaCl, 1 mM DTT, and then washed three times. The proteins bound on the resin were eluted by the same buffer supplemented with 20 mM maltose. The input and output samples were loaded to SDS-PAGE and detected by Coomassie Brilliant Blue (CBB) staining.

Bio-layer interferometry (BLI) analysis

Interaction analysis was performed using an Octet Red 96 instrument at 25 °C (ForteBio) as described previously (12). WT MST4/MOB4(53–210) protein was labeled by biotin in 20 mM HEPES, pH 7.5, 100 mM NaCl, and biotinylated proteins were immobilized on streptavidin (SA) biosensors and incubated with varying concentrations of WT or mutated MOB4(53–210)/MST4 proteins in 1× kinetics buffer (1× PBS containing 0.01% BSA and 0.002% Tween 20). Data were analyzed using Octet Data Analysis Software 7.0 (ForteBio).

ITC

ITC experiments were conducted using an iTC200 instrument from Microcal at 25 °C. For calorimetric measurements, purified MOB4(33–215) was loaded into the ITC cell at a concentration of 100 μM, and synthetic pMST4 peptides in concentrations of 1 mM were auto-loaded into the syringe. All samples were in the same buffer containing 20 mM HEPES, pH 7.5, 100 mM NaCl. Each titration included a single 0.4-μl injection followed by 19 sequential injections of 2-μl aliquots, with a spacing of 300 s between the injections, and stirring at 1000 rpm. Data were analyzed using the ORIGIN data analysis software (MicroCal Software).

Immunoprecipitation and immunoblot analysis

For immunoprecipitation experiments, whole-cell extracts of HEK293FT cells were collected 24 h after transfection or stimulation, and cells were lysed with RIPA buffer (150 mM NaCl, 100 mM Tris, pH 8.0, 1% Triton X-100, 5 mM EDTA, and 10 mM NaF) supplemented with 1 mM phenylmethylsulfonyl fluoride and the protease inhibitor mixture. After centrifugation at 12,000 rpm for 20 min at 4 °C, supernatants were collected and incubated overnight with the indicated antibodies together with protein A/G beads (Santa Cruz Biotechnology). After incubation, beads were washed and then eluted with SDS loading buffer and boiled. For immunoblot analysis, immunoprecipitates or whole-cell extracts were subjected to SDS-PAGE, transferred onto polyvinylidene difluoride membranes, and then detected with the indicated antibodies.

MTT assay

Cell proliferation rate was measured using the MTT assay according to the manufacturer's instructions (BOSTER, Wuhan, China). Briefly, PANC-1 cells were first infected with lentivirus expressing the indicated proteins for 24 h and then re-seeded in triplicate in 96-well plates at a density of 3×10^3 cells per well in 100 μl of complete media. Every 24 h after re-seeding, MTT solution was added, and cells were cultured for an additional 4 h. Formazan dye was then solubilized by dimethyl sulfoxide (DMSO), and the absorbance was measured.

Transwell migration assay

PANC-1 cells were subjected to lentivirus-mediated infection for 24 h. For transwell migration assay, 2×10^4 cells were placed on the upper layer of a cell-permeable membrane. Following an incubation of 24 h, the cells that had migrated through the membrane were stained with crystal violet and

visualized by microscope. All fields were selected in a blind manner. Cells were further eluted by a buffer containing 50% ethanol and 0.1% acetic acid, and the absorptions were detected by spectrophotometer with a wavelength at 570 nm.

Real-time PCR

Real-time PCR was performed on a Step Two Real-Time PCR System (Applied Biosystems) using the comparative C_t quantization method. Real-time PCR Master Mix (Toyobo) was used to detect and quantify the expression level of the target gene. GAPDH was used as an internal control. The primers used were as follows: CTGF, 5′-AAAAGTGCATCCGTACTCCCA-3′ (F), and 5′-CCGTCGGTACATACTCCACAG-3′ (R); BIRC5, 5′-AGGACCACCGCATCTCTACAT-3′ (F), and 5′-AAGTCTGGCTCGTTCTCAGTG-3′ (R); and GAPDH, 5′-GGCATCCTGGGCTACACTGA-3′ (F), and 5′-GAGTGGGTGTCGCTGTTGAA-3′ (R), where F is forward; R is reverse.

Tissue microarray and IHC staining

PC and healthy tissue microarray (TMA) sections were prepared by Shanghai Outdo Biotech Co., Ltd. (Shanghai, China). This tissue array contains tissues from 30 human patients containing healthy pancreas and 30 patients with PC to examine the expression profiles of MST4, MOB4, MST1, or YAP by IHC. For IHC, TMA sections were incubated with anti-MST4 (1:100 dilution), anti-MOB4 (1:50 dilution), anti-MST1 (1:20 dilution), or anti-YAP (1:50 dilution) antibody. MST4, MOB4, MST1, and YAP staining were scored by two independent pathologists, blinded to the clinical characteristics of the patients. The scoring system was based on the staining intensity and extent. Staining intensity was classified as 0 (negative), 1 (weak), 2 (moderate), and 3 (strong). Staining extent depended on the percentage of positive cells and was divided into 0 (<5%), 1 (5–25%), 2 (26–50%), 3 (51–75%), and 4 (>75%). According to the staining intensity and the staining extent scores, the IHC result was classified as 0–1, negative (−); 2–4, weakly positive (+); 5–8, moderately positive (++); and 9–12, strongly positive (+++).

Immunofluorescence assay

Cells were grown on coverslips, washed once with PBS, and fixed in 4% paraformaldehyde. After permeabilization, cells were blocked with 5% BSA and then incubated with primary antibodies. After three separate washes, cells were incubated with Alexa Fluor-conjugated secondary antibodies and then stained with DAPI. The coverslips were washed extensively and fixed on slides. Images were captured using a Leica laser-scanning confocal microscope (Leica TCS SP2 AOBS).

Statistical analysis

Statistical analysis was performed with the SAS statistical software package (9.1.3) and GraphPad Prism 7.0. Data are presented as means ± S.D. Student's *t* test was used for continuous variables. Pearson's coefficient test was used for correlation analysis. *p* values of less than 0.05 were considered statistically significant.

Accession codes

The structural coordinate of the pMST4–MOB4 complex was deposited in the PDB under the code 5YF4.

Author contributions—M. C. contributed to most of the experiments. Z. S. did structural analysis. H. Z., Y. L., X. Z., Z. G., and J. G. contributed to cellular experiments. L. Z., J. M., and Q. X. did protein purification. Y. Z. and Y. C. helped in data analysis and discussion. Z. S., M. C., and S. J. contributed to experimental design and data analysis. M. C., Z. S., S. J., and Z. Z. wrote the manuscript. Z. Z. supervised the project.

Acknowledgments—We appreciate the generous support by Professors Naihe Jing, Mofang Liu, and Jinqiu Zhou at the Shanghai Institute of Biochemistry and Cell Biology, Chinese Academy of Sciences, University of Chinese Academy of Sciences. We thank the staff from the BL19U1 beamline of the National Facility for Protein Science Shanghai (NFPS), at Shanghai Synchrotron Radiation Facility, for assistance during data collection.

References

1. Harvey, K. F., Pfleger, C. M., and Hariharan, I. K. (2003) The *Drosophila* Mst ortholog, Hippo, restricts growth and cell proliferation and promotes apoptosis. *Cell* **114,** 457–467 CrossRef Medline
2. Wu, S., Huang, J., Dong, J., and Pan, D. (2003) Hippo encodes a Ste-20 family protein kinase that restricts cell proliferation and promotes apoptosis in conjunction with salvador and warts. *Cell* **114,** 445–456 CrossRef Medline
3. Pan, D. (2007) Hippo signaling in organ size control. *Genes Dev.* **21,** 886–897 CrossRef Medline
4. Zhao, B., Lei, Q. Y., and Guan, K. L. (2008) The Hippo–YAP pathway: new connections between regulation of organ size and cancer. *Curr. Opin. Cell Biol.* **20,** 638–646 CrossRef Medline
5. Yu, F. X., Zhao, B., and Guan, K. L. (2015) Hippo pathway in organ size control, tissue homeostasis, and cancer. *Cell* **163,** 811–828 CrossRef Medline
6. Jiao, S., Wang, H., Shi, Z., Dong, A., Zhang, W., Song, X., He, F., Wang, Y., Zhang, Z., Wang, W., Wang, X., Guo, T., Li, P., Zhao, Y., Ji, H., Zhang, L., and Zhou, Z. (2014) A peptide mimicking VGLL4 function acts as a YAP antagonist therapy against gastric cancer. *Cancer Cell* **25,** 166–180 CrossRef Medline
7. Praskova, M., Xia, F., and Avruch, J. (2008) MOBKL1A/MOBKL1B phosphorylation by MST1 and MST2 inhibits cell proliferation. *Curr. Biol.* **18,** 311–321 CrossRef Medline
8. Ni, L., Zheng, Y., Hara, M., Pan, D., and Luo, X. (2015) Structural basis for Mob1-dependent activation of the core Mst-Lats kinase cascade in Hippo signaling. *Genes Dev.* **29,** 1416–1431 CrossRef Medline
9. Hergovich, A., Schmitz, D., and Hemmings, B. A. (2006) The human tumour suppressor LATS1 is activated by human MOB1 at the membrane. *Biochem. Biophys. Res. Commun.* **345,** 50–58 CrossRef
10. Huang, J., Wu, S., Barrera, J., Matthews, K., and Pan, D. (2005) The Hippo signaling pathway coordinately regulates cell proliferation and apoptosis by inactivating Yorkie, the *Drosophila* homolog of YAP. *Cell* **122,** 421–434 CrossRef Medline
11. Ma, X., Zhao, H., Shan, J., Long, F., Chen, Y., Chen, Y., Zhang, Y., Han, X., and Ma, D. (2007) PDCD10 interacts with Ste20-related kinase MST4 to promote cell growth and transformation via modulation of the ERK pathway. *Mol. Biol. Cell* **18,** 1965–1978 CrossRef Medline
12. Shi, Z., Jiao, S., Zhang, Z., Ma, M., Zhang, Z., Chen, C., Wang, K., Wang, H., Wang, W., Zhang, L., Zhao, Y., and Zhou, Z. (2013) Structure of the MST4 in complex with MO25 provides insights into its activation mechanism. *Structure* **21,** 449–461 CrossRef Medline
13. Thompson, B. J., and Sahai, E. (2015) MST kinases in development and disease. *J. Cell Biol.* **210,** 871–882 CrossRef Medline

14. Cho, C. Y., Lee, K. T., Chen, W. C., Wang, C. Y., Chang, Y. S., Huang, H. L., Hsu, H. P., Yen, M. C., Lai, M. Z., and Lai, M. D. (2016) MST3 promotes proliferation and tumorigenicity through the VAV2/Rac1 signal axis in breast cancer. *Oncotarget* **7,** 14586–14604 CrossRef Medline
15. Huang, C. Y., Wu, Y. M., Hsu, C. Y., Lee, W. S., Lai, M. D., Lu, T. J., Huang, C. L., Leu, T. H., Shih, H. M., Fang, H. I., Robinson, D. R., Kung, H. J., and Yuan, C. J. (2002) Caspase activation of mammalian sterile 20-like kinase 3 (Mst3). Nuclear translocation and induction of apoptosis. *J. Biol. Chem.* **277,** 34367–34374 CrossRef Medline
16. Tang, F., Zhang, L., Xue, G., Hynx, D., Wang, Y., Cron, P. D., Hundsrucker, C., Hergovich, A., Frank, S., Hemmings, B. A., and Schmitz-Rohmer, D. (2014) hMOB3 modulates MST1 apoptotic signaling and supports tumor growth in glioblastoma multiforme. *Cancer Res.* **74,** 3779–3789 CrossRef Medline
17. Dan, I., Watanabe, N. M., and Kusumi, A. (2001) The Ste20 group kinases as regulators of MAP kinase cascades. *Trends Cell Biol.* **11,** 220–230 CrossRef Medline
18. Goudreault, M., D'Ambrosio, L. M., Kean, M. J., Mullin, M. J., Larsen, B. G., Sanchez, A., Chaudhry, S., Chen, G. I., Sicheri, F., Nesvizhskii, A. I., Aebersold, R., Raught, B., and Gingras, A. C. (2009) A PP2A phosphatase high density interaction network identifies a novel striatin-interacting phosphatase and kinase complex linked to the cerebral cavernous malformation 3 (CCM3) protein. *Mol. Cell. Proteomics* **8,** 157–171 CrossRef Medline
19. Shi, Z., Jiao, S., and Zhou, Z. (2016) STRIPAK complexes in cell signaling and cancer. *Oncogene* **35,** 4549–4557 CrossRef Medline
20. Hwang, J., and Pallas, D. C. (2014) STRIPAK complexes: structure, biological function, and involvement in human diseases. *Int. J. Biochem. Cell Biol.* **47,** 118–148 CrossRef Medline
21. Baillat, G., Moqrich, A., Castets, F., Baude, A., Bailly, Y., Benmerah, A., and Monneron, A. (2001) Molecular cloning and characterization of phocein, a protein found from the Golgi complex to dendritic spines. *Mol. Biol. Cell* **12,** 663–673 CrossRef Medline
22. Haeberlé, A. M., Castets, F., Bombarde, G., Baillat, G., and Bailly, Y. (2006) Immunogold localization of phocein in dendritic spines. *J. Comp. Neurol.* **495,** 336–350 CrossRef Medline
23. Madsen, C. D., Hooper, S., Tozluoglu, M., Bruckbauer, A., Fletcher, G., Erler, J. T., Bates, P. A., Thompson, B., and Sahai, E. (2015) STRIPAK components determine mode of cancer cell migration and metastasis. *Nat. Cell Biol.* **17,** 68–80 CrossRef Medline
24. Qiao, M., Wang, Y., Xu, X., Lu, J., Dong, Y., Tao, W., Stein, J., Stein, G. S., Iglehart, J. D., Shi, Q., and Pardee, A. B. (2010) Mst1 is an interacting protein that mediates PHLPPs' induced apoptosis. *Mol. Cell* **38,** 512–523 CrossRef Medline
25. ten Klooster, J. P., Jansen, M., Yuan, J., Oorschot, V., Begthel, H., Di Giacomo, V., Colland, F., de Koning, J., Maurice, M. M., Hornbeck, P., and Clevers, H. (2009) Mst4 and Ezrin induce brush borders downstream of the Lkb1/Strad/Mo25 polarization complex. *Dev. cell* **16,** 551–562 CrossRef Medline
26. Gloerich, M., ten Klooster, J. P., Vliem, M. J., Koorman, T., Zwartkruis, F. J., Clevers, H., and Bos, J. L. (2012) Rap2A links intestinal cell polarity to brush border formation. *Nat. Cell Biol.* **14,** 793–801 CrossRef Medline
27. Sung, V., Luo, W., Qian, D., Lee, I., Jallal, B., and Gishizky, M. (2003) The Ste20 kinase MST4 plays a role in prostate cancer progression. *Cancer Res.* **63,** 3356–3363 Medline
28. Huang, T., Kim, C. K., Alvarez, A. A., Pangeni, R. P., Wan, X., Song, X., Shi, T., Yang, Y., Sastry, N., Horbinski, C. M., Lu, S., Stupp, R., Kessler, J. A., Nishikawa, R., Nakano, I., *et al.* (2017) MST4 Phosphorylation of ATG4B regulates autophagic activity, tumorigenicity, and radioresistance in glioblastoma. *Cancer Cell* **32,** 840–855.e8 CrossRef Medline
29. Preisinger, C., Short, B., De Corte, V., Bruyneel, E., Haas, A., Kopajtich, R., Gettemans, J., and Barr, F. A. (2004) YSK1 is activated by the Golgi matrix protein GM130 and plays a role in cell migration through its substrate 14-3-3ζ. *J. Cell Biol.* **164,** 1009–1020 CrossRef Medline
30. Fidalgo, M., Fraile, M., Pires, A., Force, T., Pombo, C., and Zalvide, J. (2010) CCM3/PDCD10 stabilizes GCKIII proteins to promote Golgi assembly and cell orientation. *J. Cell Sci.* **123,** 1274–1284 CrossRef Medline
31. Kean, M. J., Ceccarelli, D. F., Goudreault, M., Sanches, M., Tate, S., Larsen, B., Gibson, L. C., Derry, W. B., Scott, I. C., Pelletier, L., Baillie, G. S., Sicheri, F., and Gingras, A. C. (2011) Structure-function analysis of core STRIPAK Proteins: a signaling complex implicated in Golgi polarization. *J. Biol. Chem.* **286,** 25065–25075 CrossRef Medline
32. Gordon, J., Hwang, J., Carrier, K. J., Jones, C. A., Kern, Q. L., Moreno, C. S., Karas, R. H., and Pallas, D. C. (2011) Protein phosphatase 2a (PP2A) binds within the oligomerization domain of striatin and regulates the phosphorylation and activation of the mammalian Ste20-Like kinase Mst3. *BMC Biochem.* **12,** 54 CrossRef Medline
33. Ribeiro, P. S., Josué, F., Wepf, A., Wehr, M. C., Rinner, O., Kelly, G., Tapon, N., and Gstaiger, M. (2010) Combined functional genomic and proteomic approaches identify a PP2A complex as a negative regulator of Hippo signaling. *Mol. Cell* **39,** 521–534 CrossRef Medline
34. Couzens, A. L., Knight, J. D., Kean, M. J., Teo, G., Weiss, A., Dunham, W. H., Lin, Z. Y., Bagshaw, R. D., Sicheri, F., Pawson, T., Wrana, J. L., Choi, H., and Gingras, A. C. (2013) Protein interaction network of the mammalian Hippo pathway reveals mechanisms of kinase-phosphatase interactions. *Sci. Signal.* **6,** rs15 CrossRef Medline
35. Bae, S. J., Ni, L., Osinski, A., Tomchick, D. R., Brautigam, C. A., and Luo, X. (2017) SAV1 promotes Hippo kinase activation through antagonizing the PP2A phosphatase STRIPAK. *Elife* **6,** e30278 CrossRef Medline
36. Jiao, S., Zhang, Z., Li, C., Huang, M., Shi, Z., Wang, Y., Song, X., Liu, H., Li, C., Chen, M., Wang, W., Zhao, Y., Jiang, Z., Wang, H., Wong, C. C., *et al.* (2015) The kinase MST4 limits inflammatory responses through direct phosphorylation of the adaptor TRAF6. *Nat. Immunol.* **16,** 246–257 CrossRef Medline
37. Zhang, M., Dong, L., Shi, Z., Jiao, S., Zhang, Z., Zhang, W., Liu, G., Chen, C., Feng, M., Hao, Q., Wang, W., Yin, M., Zhao, Y., Zhang, L., and Zhou, Z. (2013) Structural mechanism of CCM3 heterodimerization with GCKIII kinases. *Structure* **21,** 680–688 CrossRef Medline
38. Stavridi, E. S., Harris, K. G., Huyen, Y., Bothos, J., Verwoerd, P. M., Stayrook, S. E., Pavletich, N. P., Jeffrey, P. D., and Luca, F. C. (2003) Crystal structure of a human Mob1 protein: toward understanding Mob-regulated cell cycle pathways. *Structure* **11,** 1163–1170 CrossRef Medline
39. Zhao, X., Wang, X., Fang, L., Lan, C., Zheng, X., Wang, Y., Zhang, Y., Han, X., Liu, S., Cheng, K., Zhao, Y., Shi, J., Guo, J., Hao, J., Ren, H., and Nie, G. (2017) A combinatorial strategy using YAP and pan-RAF inhibitors for treating KRAS-mutant pancreatic cancer. *Cancer Lett.* **402,** 61–70 CrossRef Medline
40. Li, X., Liu, Y., Zhang, C., Niu, Q., Wang, H., Che, C., Xie, M., Zhou, B., Xu, Y., Zhang, Q., Wu, J., and Tian, Z. (2017) *Stiehopus japonieus* acidic mucopolysaccharide inhibits the proliferation of pancreatic cancer SW1990 cells through Hippo–YAP pathway. *Oncotarget* **8,** 16356–16366 CrossRef Medline
41. Yuan, Y., Li, D., Li, H., Wang, L., Tian, G., and Dong, Y. (2016) YAP overexpression promotes the epithelial-mesenchymal transition and chemoresistance in pancreatic cancer cells. *Mol. Med. Rep.* **13,** 237–242 CrossRef Medline
42. Gomez, M., Gomez, V., and Hergovich, A. (2014) The Hippo pathway in disease and therapy: cancer and beyond. *Clin. Transl. Med.* **3,** 22 CrossRef Medline
43. Song, H., Mak, K. K., Topol, L., Yun, K., Hu, J., Garrett, L., Chen, Y., Park, O., Chang, J., Simpson, R. M., Wang, C. Y., Gao, B., Jiang, J., and Yang, Y. (2010) Mammalian Mst1 and Mst2 kinases play essential roles in organ size control and tumor suppression. *Proc. Natl. Acad. Sci. U.S.A.* **107,** 1431–1436 CrossRef Medline
44. Avruch, J., Zhou, D., Fitamant, J., Bardeesy, N., Mou, F., and Barrufet, L. R. (2012) Protein kinases of the Hippo pathway: regulation and substrates. *Semin. Cell Dev. Biol.* **23,** 770–784 CrossRef Medline
45. Schroeder, M. C., and Halder, G. (2012) Regulation of the Hippo pathway by cell architecture and mechanical signals. *Semin. Cell Dev. Biol.* **23,** 803–811 CrossRef Medline
46. Rock, J. M., Lim, D., Stach, L., Ogrodowicz, R. W., Keck, J. M., Jones, M. H., Wong, C. C., Yates, J. R., 3rd., Winey, M., Smerdon, S. J., Yaffe, M. B., and Amon, A. (2013) Activation of the yeast Hippo pathway by phosphorylation-dependent assembly of signaling complexes. *Science* **340,** 871–875 CrossRef Medline

47. Yuan, P., He, X. H., Rong, Y. F., Cao, J., Li, Y., Hu, Y. P., Liu, Y., Li, D., Lou, W., and Liu, M. F. (2017) KRAS/NF-κB/YY1/miR-489 signaling axis controls pancreatic cancer metastasis. *Cancer Res.* **77,** 100–111 CrossRef Medline
48. Otwinowski, Z., and Minor, W. (1997) Processing of X-ray diffraction data collected in oscillation mode. *Methods Enzymol.* **276,** 307–326 CrossRef Medline
49. Emsley, P., Lohkamp, B., Scott, W. G., and Cowtan, K. (2010) Features and development of Coot. *Acta Crystallogr. D Biol. Crystallogr.* **66,** 486–501 CrossRef Medline
50. Adams, P. D., Afonine, P. V., Bunkóczi, G., Chen, V. B., Davis, I. W., Echols, N., Headd, J. J., Hung, L.-W., Kapral, G. J., Grosse-Kunstleve, R. W., McCoy, A. J., Moriarty, N. W., Oeffner, R., Read, R. J., Richardson, D. C., *et al.* (2010) PHENIX: a comprehensive Python-based system for macromolecular structure solution. *Acta Crystallogr. D Biol. Crystallogr.* **66,** 213–221 CrossRef Medline
51. Winn, M. D., Ballard, C. C., Cowtan, K. D., Dodson, E. J., Emsley, P., Evans, P. R., Keegan, R. M., Krissinel, E. B., Leslie, A. G., McCoy, A., McNicholas, S. J., Murshudov, G. N., Pannu, N. S., Potterton, E. A., Powell, H. R., *et al.* (2011) Overview of the CCP4 suite and current developments. *Acta Crystallogr. D Biol. Crystallogr.* **67,** 235–242 CrossRef Medline
52. Collaborative Computational Project, No. 4. (1994) The CCP4 suite: programs for protein crystallography. *Acta Crystallogr. D Biol. Crystallogr.* **50,** 760–763 CrossRef Medline
53. Tang, Z., Li, C., Kang, B., Gao, G., Li, C., and Zhang, Z. (2017) GEPIA: A web server for cancer and normal gene expression profiling and interactive analyses. *Nucleic Acids Res.* **45,** W98–W102 CrossRef Medline